AGU PUBLICATIONS

Geophysical Research Letters

RESEARCH LETTER
10.1002/2016GL071339

Key Points:
- Models with the same large-scale flow can have very different tropospheric transport
- This is mainly due to large differences in parameterized convective transport
- Transport differences between free-running models are smaller because parameterized convection is more similar

Correspondence to:
C. Orbe,
clara.orbe@nasa.gov

Citation:
Orbe, C., D. W. Waugh, H. Yang, J.-F. Lamarque, S. Tilmes, and D. E. Kinnison (2016), Tropospheric transport differences between models using the same large-scale meteorological fields, *Geophys. Res. Lett.*, *44*, doi:10.1002/2016GL071339.

Received 28 SEP 2016
Accepted 2 DEC 2016
Accepted article online 6 DEC 2016

Tropospheric transport differences between models using the same large-scale meteorological fields

Clara Orbe[1,2], Darryn W. Waugh[2], Huang Yang[2], Jean-Francois Lamarque[3], Simone Tilmes[3], and Douglas E. Kinnison[3]

[1]Global Modeling and Assimilation Office, NASA Goddard Space Flight Center, Greenbelt, Maryland, USA, [2]Department of Earth and Planetary Sciences, The Johns Hopkins University, Baltimore, Maryland, USA, [3]National Center for Atmospheric Research, Atmospheric Chemistry Observations and Modeling Laboratory, Boulder, Colorado, USA

Abstract The transport of chemicals is a major uncertainty in the modeling of tropospheric composition. A common approach is to transport gases using the winds from meteorological analyses, either using them directly in a chemical transport model or by constraining the flow in a general circulation model. Here we compare the transport of idealized tracers in several different models that use the same meteorological fields taken from Modern-Era Retrospective analysis for Research and Applications (MERRA). We show that, even though the models use the same meteorological fields, there are substantial differences in their global-scale tropospheric transport related to large differences in parameterized convection between the simulations. Furthermore, we find that the transport differences between simulations constrained with the same-large scale flow are larger than differences between free-running simulations, which have differing large-scale flow but much more similar convective mass fluxes. Our results indicate that more attention needs to be paid to convective parameterizations in order to understand large-scale tropospheric transport in models, particularly in simulations constrained with analyzed winds.

1. Introduction

One major uncertainty in the modeling of tropospheric composition is the transport of chemicals. One approach to reducing this uncertainty is to transport trace gases and aerosols using winds from meteorological analyses, either using them directly in a chemical transport model (CTM) or by constraining the flow in a general circulation model (GCM). In either case, it is assumed that modeled constituents will be more faithfully representative of the atmospheric conditions of a given time period when analyzed winds are used, compared to when the meteorological fields come from a free-running model (i.e., not constrained to an analysis). However, because of the various ways in which a model may be constrained with analyzed fields, this is far from obvious. In fact, studies on stratospheric transport have long shown that the accuracy of transport computations using analyzed winds is questionable, either because of misrepresentations of the residual circulation [e.g., *Meijer et al.*, 2004] or because of anomalous transport resulting from excessive mixing [e.g., *Schoeberl et al.*, 2003; *Pawson et al.*, 2007].

In addition to uncertainties associated with using analyzed winds, parameterizations in models, e.g., deep convection, gravity wave drag, and the planetary boundary layer, represent large sources of uncertainty in tropospheric transport [e.g., *Lawrence et al.*, 2003; *Doherty et al.*, 2005; *Rind et al.*, 2007]. For example, *Gilliland and Hartley* [1998] showed that rates of interhemispheric exchange differed by nearly ~35% between two versions of the same model using different convective parameterizations. More recently, intercomparisons between CTMs show that uncertainties in (parameterized) convective transport contribute to large intermodel differences in global methane and various very short lived ozone depleting substances [*Hossaini et al.*, 2016], among other constituents [*Patra et al.*, 2011; *Saito et al.*, 2013]. There are also large differences in convective transport between general circulation models, despite the fact that they all use similar parameterizations based on the mass flux approach, both because different closures are used and because of the large range in the behavior of convection that can occur within a single parameterization [*Scinocca and McFarlane*, 2004; *Ott et al.*, 2011]. Because of additional choices that must be made in representing parameterized convection in simulations using analyzed winds—be it by obtaining the convective mass fluxes directly from the analysis data set or by recalculating them using the model's own convective parameterization—it is not obvious that using specified winds should necessarily reduce transport uncertainties but rather may amplify them.

One way to distinguish between the uncertainties associated with parameterized convection versus uncertainties associated with the prescribed analyzed meteorological fields is to compare simulations that are driven with the same large-scale flow. In this study, we control for differences in the large-scale flow by comparing simulations between models that are all driven with the same analyzed winds. Our first goal is to document the large-scale tropospheric transport differences between the simulations. The second goal is to interpret these differences in terms of the models' subgrid scale transport. We also examine how these differences compare with the large-scale transport differences between simulations that use internally generated meteorological fields (i.e., different large-scale flow). The model integrations used comprise a small subset of experiments that were performed as part of the joint International Global Atmospheric Chemisty/Stratospheric Processes and their Role in Climate Chemistry-Climate Model Initiative (CCMI) [*Eyring et al.*, 2013; *Morgenstern et al.*, 2016].

We diagnose tropospheric transport using idealized tracers that were also requested as model output in the CCMI simulations and that provide tracer-independent diagnostics of the flow that do not reflect intermodel differences in prescribed chemical emissions or reactions. These include three tracers that quantify transport from the Northern Hemisphere (NH) midlatitude surface as well as one tracer that assesses the exchange between the stratosphere and the troposphere (Table 1b). Following a brief exposition of the methodology in section 2 we present results in section 3, followed by conclusions in section 4.

2. Methods

2.1. Model Simulations

The six simulations compared in this study are listed in Table 1a. All simulations were performed at comparable horizontal resolutions and with model tops at or above the mesosphere. Four of the integrations are all forced with the same large-scale meteorological fields, which are taken from Modern-Era Retrospective analysis for Research and Applications (MERRA) for the years 1980–2009 [*Rienecker et al.*, 2011]. They comprise two suites of simulations using MERRA: one suite consisting of two simulations produced from models developed at NASA Goddard Space Flight Center and the other suite consisting of two simulations produced from models developed under the Community Earth System Model framework and run by the National Center for Atmospheric Research (NCAR). The first simulation in the NASA MERRA suite, hereafter referred to as the NASA-CTM simulation, uses the NASA Global Modeling Initiative (GMI) three-dimensional chemical transport model [*Strahan et al.*, 2007] and is the same simulation that was used in *Waugh et al.* [2013] and *Orbe et al.* [2016]. The convective mass fluxes used in the GMI CTM are taken directly from the MERRA assimilated fields and, therefore, reflect the Relaxed-Arakawa Schubert (RAS) convection scheme [*Moorthi and Suarez*, 1992] of the original GCM (Goddard Earth Observing System version 5 (GEOS-5)) that produced MERRA. RAS is a mass flux scheme with an updraft only detraining plume cloud model and a quasi-equilibrium closure.

The second NASA MERRA simulation, denoted throughout as NASA-SD, is generated by the online version of the GEOS-5 GCM [*Suarez et al.*, 2008] run in "replay" mode, wherein the model is adjusted to MERRA analysis zonal and meridional winds, temperature, and surface pressure and recalculates the rest of the physics and dynamical quantities using the same incremental analysis update technique that is used to generate the MERRA assimilation [*Bloom et al.*, 1996]. Note that, unlike the CTM simulation, which uses the three-hourly averaged assimilated fields from MERRA, the NASA-SD simulation replays to the MERRA analysis fields at every synoptic time (00, 06, 12, and 18 UT). By construction, therefore, a GEOS-5 replay simulation that is made with an identical version of the model used to produce MERRA would generate the analysis meteorology exactly and has been used in previous studies to examine aerosols and trace gases like carbon monoxide [e.g., *Colarco et al.*, 2010; *Strode et al.*, 2015]. The convective mass fluxes are recalculated by the model and, therefore, reflect the convective parameterization in its current version of the model, which has changed in several ways since MERRA was originally produced. That said, while the underlying RAS scheme has been updated in recent versions of the model these changes have applied only to the parameters within the scheme and do not mark a fundamental change in the parameterization [*Molod et al.*, 2012]. Note that, while two different models were used to produce the NASA-CTM and NASA-SD simulations, the large-scale tropospheric transport properties between the models are very similar, as shown in section 4. For the sake of brevity, therefore, they are referred to as simply the "NASA" MERRA simulations.

The NCAR-MERRA suite consists of two nudged simulations of the Whole Atmosphere Community Climate Model (WACCM) [*Marsh et al.*, 2013]. Specifically, WACCM is constrained by MERRA temperature, surface pressure, and zonal and meridional winds using the approach described in *Kunz et al.* [2011] with relaxation time

Table 1a. Details of the Model Integrations, Where Columns 3–6 Correspond to the Horizontal Resolution, Number of Vertical Levels and Model Top, Source of Meteorological Fields, and Reference for the Model's Convective Parameterizations[a]

		Model Experiments			
Simulation Name	Model (Reference)	Horizontal Resolution	Vertical Levels (Model Top)	Large-Scale Flow	Convective Parameterization
NASA-CTM	NASA Global Modeling Initiative CTM [*Strahan et al.*, 2007]	2° × 2.5°	72 (0.01 hPa)	MERRA	*Moorthi and Suarez* [1992]
NASA-SD	Goddard Earth Observing System, Version 5 (GEOS-5) GCM [*Suarez et al.*, 2008]	" "	" "	MERRA	" "
NASA-FR	" "	" "	" "	Free-running	" "
NCAR-SD-5hr	Whole Atmosphere Community Climate Model (WACCM) [*Marsh et al.*, 2013]	1.9° × 2.5°	88 (145 km)	MERRA	*Hack* [1994] *Zhang and McFarlane* [1995]
NCAR-SD-50hr	" "	" "	" "	MERRA	" "
NCAR-FR	" "	" "	" "	Free-running	" "

[a]Four simulations comprise the NASA and NCAR MERRA suites of simulations (rows 1–2, 4–5), all driven with MERRA meteorological fields for years 1980–2009. In addition to the MERRA simulations, two free-running (FR) simulations are performed in which GEOS-5 and WACCM use internally generated meteorological fields, referred to as the NASA-FR and NCAR-FR simulations, respectively (rows 3 and 6).

constants of 5 h and 50 h for the NCAR-SD-5hr and NCAR-SD-50hr simulations, respectively. The convective mass fluxes in the NCAR-SD simulations are not taken from MERRA but rather derived from the Community Atmosphere Model (CAM) Version 4.0 physics, which represents deep convection using the parameterizations of *Zhang and McFarlane* [1995] and *Hack* [1994] for deep and shallow convection, respectively. (Note that we have performed an analysis using identical tracer output from CAM4 and find only negligible tropospheric transport differences with the WACCM simulations presented here.)

Finally, in addition to the MERRA suites of simulations, we also analyze a suite consisting of two free-running (FR) simulations of GEOS-5 and WACCM, in which the meteorological fields are internally generated. Both simulations use the same sea surface temperatures and sea ice concentrations, prescribed as monthly mean boundary conditions from the Hadley Centre Sea Ice and Sea Surface Temperature data set Version 1 (HadISST1) data set provided by the UK Met Office Hadley Centre [*Rayner et al.*, 2003]. Note that both the NASA-FR and NCAR-FR simulations were generated using the exact same model versions that were used to produce the NASA-SD and NCAR-SD simulations, respectively.

2.2. Idealized Tracers

With the exception of the stratosphere-troposphere-exchange (STE) tracer χ_{STE}, all of the tracers examined in this study, shown in Table 1b, are identical to the tracers presented in *Orbe et al.* [2016]. The first three tracers' boundary conditions are zonally uniform and are defined over the same NH surface region over mid-latitudes, Ω_{MID}, defined as the first model level spanning all grid points between 30°N and 50°N. The first two

Table 1b. All of the Tracers (χ) Integrated in the Simulations Satisfy the Tracer Continuity Equation, $(\partial_t + \mathcal{T})\chi(\mathbf{r}, t|\Omega) = S$ in the Interior of the Atmosphere (That Is, Outside of Ω), Where $\mathcal{T}$ Is the Linear Advection-Diffusion Transport Operator and S Denotes Interior Sources and Sinks[a]

	Idealized Tracers	
Tracer (χ)	Boundary Condition (χ_Ω)	Source (S)
5 day NH loss (χ_5)	1	$-\chi/\tau_c$ (τ_c = 5 days; entire atmosphere)
50 day NH loss (χ_{50})	1	$-\chi/\tau_c$ (τ_c = 50 days; entire atmosphere)
Mean age (Γ)	0	1 year/year
Stratospheric loss (χ_{STE})	200 ppbv above 80 hPa	$-\chi/\tau_c$ (τ_c = 25 days; troposphere only)

[a]For the first three tracers (rows 2–4) Ω is taken to be the NH midlatitude surface, Ω_{MID}, which is defined throughout as the first model level spanning latitudes between 30°N and 50°N. By comparison, the STE tracer, χ_{STE}, is set to 200 ppbv for pressures less than and equal to 80 mb and decays uniformly in the troposphere at a loss rate $\tau_d = 25$ days^{-1} (row 4).

tracers, referred to throughout as the 5 day and 50 day idealized loss tracers (χ_5 and χ_{50}) are fixed to a value of 100 ppbv over Ω_{MID} and undergo spatially uniform exponential loss at rates of 5 days^{-1} and 50 days^{-1}, respectively.

We also carry an idealized "NH clock" or ideal age tracer (e.g., Thiele and Sarmiento (1990)), which is initially set to a value of zero throughout the troposphere; thereafter, it is held to zero over Ω_{MID} and subject to a constant aging of 1 year/year in the rest of the model surface layer and throughout the atmosphere [*Waugh et al.*, 2013]. The statistically stationary value of $\Gamma(\mathbf{r}|\Omega_{MID})$, the mean age, is equal to the average time since the air at a region $\mathbf{r}$ in the troposphere last contacted the NH midlatitude surface Ω_{MID}, and provides a richer description of transport compared to hemispherically integrated transport quantities like the interhemispheric exchange time [*Levin and Hesshaimer*, 1996; *Geller et al.*, 1997].

The fourth tracer, χ_{STE}, which is set to a constant value of 200 ppbv above 80 mb and undergoes spatially uniform exponential loss at a rate of 25 days^{-1}, is similar in spirit to other tracers that have been examined in previous studies, including stratosphere-to-troposphere air mass origin tracers [*Orbe et al.*, 2013] and the e90 tracer defined in *Prather et al.* [2011]. Note that our focus is on seasonal averages over December–February (DJF) and June–August (JJA), and 10 year climatological means over the time period 2000–2009, denoted throughout using the overbars. Statistical significance of the differences between all climatological mean quantities, relative to internal variability, is assessed using $\pm\sigma_\chi$, where σ denotes the standard deviation of each seasonal mean tracer (or dynamical field) over the climatological averaging period.

3. Large-Scale Tropospheric Transport

3.1. Comparisons Between MERRA Simulations

We begin by comparing the 5 day and 50 day idealized loss tracers, $\overline{\chi_5}$ and $\overline{\chi_{50}}$ (Figure 1) between the MERRA simulations. During winter, $\overline{\chi_5}^{DJF}$ and $\overline{\chi_{50}}^{DJF}$ decrease poleward away from the midlatitude source region, Ω_{MID}, roughly along potential temperature surfaces that extend into the middle and upper troposphere at high latitudes. Whereas $\overline{\chi_5}$ is mainly confined to the NH extratropics, large values of $\overline{\chi_{50}}$ span the NH subtropics and deep tropics, where they reflect low-level convergence and mean ascent associated with the Hadley circulation. During boreal summer, the patterns of $\overline{\chi_5}^{JJA}$ and $\overline{\chi_{50}}^{JJA}$ extend higher into the upper troposphere over midlatitudes, consistent both with weaker isentropic transport from northern latitudes and stronger convection over the continents [*Klonecki et al.*, 2003; *Stohl*, 2006; *Orbe et al.*, 2015].

Comparing the idealized loss tracers between the MERRA simulations, we find overall larger values of $\overline{\chi_5}$ and $\overline{\chi_{50}}$ in the NASA MERRA runs compared to the NCAR MERRA simulations, indicating more rapid transport northward to high latitudes and equatorward into the subtropics and tropics.

During winter, the differences in $\overline{\chi_5}^{DJF}$ are relatively small over the middle and poleward edge of the source region but grow moving both equatorward and poleward to high latitudes, where they are ~10% larger in the NASA-CTM and NASA-SD simulations (Figure 2a). The differences between the MERRA simulations in the NH are even larger during summer, with ~20–30% larger values of $\overline{\chi_5}^{JJA}$ in the NASA MERRA simulations (Figures 2e and 2f).

In addition to the large differences in $\overline{\chi_5}^{JJA}$ that occur at high latitudes, some of the largest differences between the NASA and NCAR MERRA suites of simulations occurs over the NH subtropics and tropics, where values of $\overline{\chi_{50}}^{DJF}$ in the NASA-CTM and NASA-SD simulations are ~30% larger than in the NCAR MERRA simulations (Figure 2b). These differences are also reflected in the mean age $\overline{\Gamma}$, which is much younger throughout the tropics and Southern Hemisphere (SH) in the NASA MERRA simulations during both winter and summer (i.e., younger ages corresponding to higher tracer concentrations) (Figure 1). That is, $\overline{\Gamma}$, which is ~0.25 years in the NH extratropical lower troposphere in all the MERRA simulations, increases to ~2.5 years over SH high latitudes in the NCAR MERRA runs, compared to ~2 years in the NASA-CTM and NASA-SD integrations (Figure 2c). Note that, while the NASA MERRA simulations are younger relative to the NCAR MERRA simulations, the modeled mean age at SH high latitudes is still larger than observational estimates inferred from SF_6 [*Waugh et al.*, 2013].

Interestingly, the differences in $\overline{\Gamma}$ arise sharply south of the origin region Ω_{MID}, where the largest meridional gradients in the mean age occur over the NH subtropics and deep tropics (Figure 1). The differences in $\overline{\Gamma}$, however, remain approximately constant over southern latitudes, which indicates that they primarily reflect differences in the tropical and subtropical lower troposphere and not differences in transport from the lower stratosphere between the MERRA simulations. To pursue this point further, we look next at $\overline{\chi}_{STE}$ (Figure 1b,

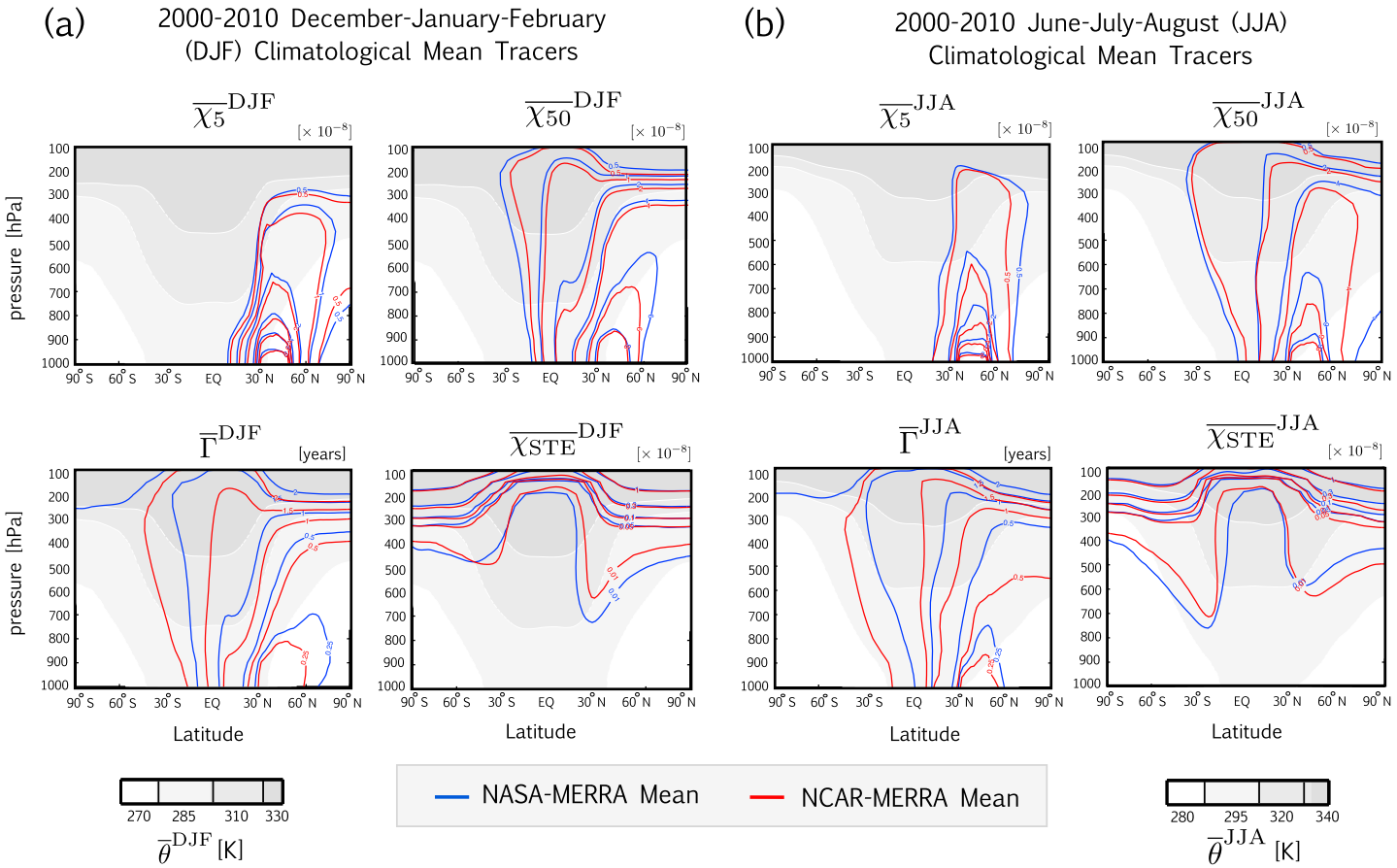

Figure 1. Climatological mean of (a) December–February (DJF) and (b) June–August (JJA) zonally averaged distributions of the 5 day and 50 day loss tracers, $\overline{\chi_5}$ and $\overline{\chi_{50}}$ (Figure 1, top); the mean age Γ (Figures 1a, bottom left, and 1b, bottom left); and the STE tracer χ_{STE} (Figures 1a, bottom right, and 1b, bottom right). The mean of the NASA and NCAR suites' model simulations, all forced with MERRA meteorological fields, are shown in the blue and red lines, respectively. Climatological seasonal mean dry potential temperature is shown in the grey contours, averaged over all of the simulations. All climatologies are performed over years 2000–2009.

bottom right), which for both seasons features strong vertical gradients in the lower stratosphere and weaker gradients in the subtropical upper troposphere, as tracer contours slope isentropically downward into the tropospheric middle world. Above 300 mb, where most of the tracer mass (~90%) resides, the differences between the NCAR and NASA MERRA simulations are very small, which indicates that the net air mass flux from the middle stratosphere into the high-latitude lower stratosphere is very similar between the simulations (Figure 1b, bottom). This indicates that the large transport differences between the NASA and NCAR MERRA simulations captured by the idealized loss and mean age tracers are not primarily the result of differences in stratosphere-troposphere exchange but rather differences in the troposphere.

3.2. Comparisons Between FR Simulations

The large-scale transport differences captured by the idealized loss and mean age tracers are much smaller between the FR simulations than between the MERRA simulations (Figure 2). During winter, the zonal mean distributions of $\overline{\chi_5}^{DJF}$ and $\overline{\chi_{50}}^{DJF}$ are nearly identical between the FR simulations, with only a slight indication of slower transport in the NCAR-FR simulation over NH high latitudes. During summer, the differences between $\overline{\chi_5}^{JJA}$ and $\overline{\chi_{50}}^{JJA}$ are relatively larger (10%) but still weak and are confined only to latitudes right over the source region.

Perhaps most striking is the excellent agreement in $\overline{\Gamma}$ between the free-running simulations, especially over southern high latitudes, where the MERRA suites of simulations differ by ~30% during both summer and winter (Figures 2c, right, and 2g, right). In fact, $\overline{\chi}_{STE}$ is the only tracer that features any statistically significant differences between the free-running simulations, with systematically larger values in the NCAR-FR simulation indicating too strong stratosphere-troposphere exchange in that model. This is consistent with, and perhaps

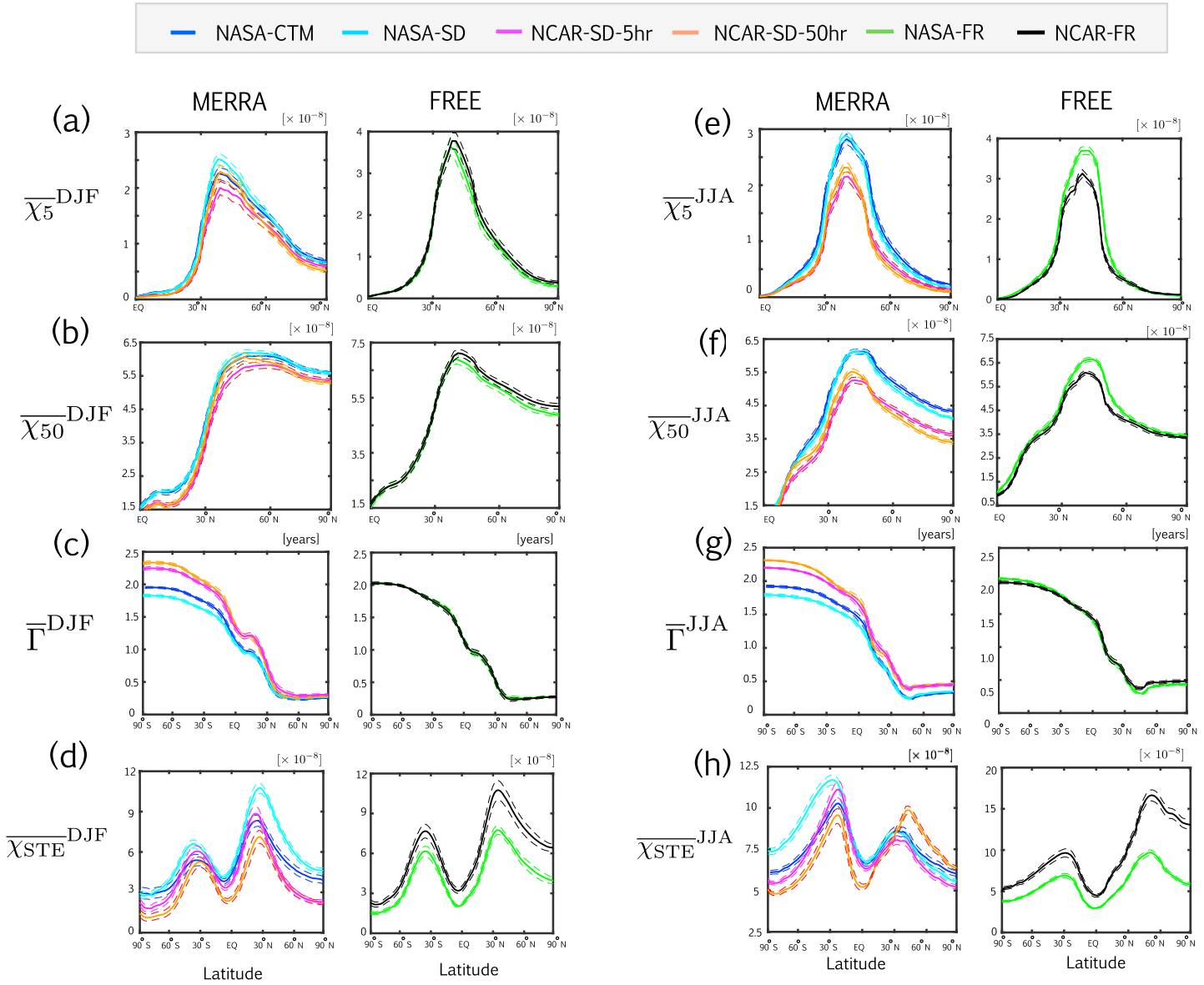

Figure 2. Latitude profiles of the 500–800 hPa zonally averaged (a–d) DJF and (e–h) JJA 5 day and 50 day loss tracers, $\overline{\chi_5}$ and $\overline{\chi_{50}}$ (Figures 2a, 2b, 2e, and 2f); the mean age Γ (Figures 2c and 2g); and the STE tracer χ_{STE} (Figures 2d and 2h). Comparisons between the (Figures 2a–2d) MERRA constrained and (Figures 2e–2h) free-running simulations, respectively. All members within each MERRA and FR suite are shown: NASA-CTM (blue), NASA-SD (cyan), NCAR-SD-5hr (pink), NCAR-SD-50hr (orange), NASA-FR (green), and NCAR-FR (black). For all simulations, the dashed lines denote $\pm\sigma_\chi$ for each tracer χ, where σ is the standard deviation of each seasonal mean calculated over the 2000–2009 climatological averaging period. Note that x axis differs between the figure panels.

related to, the high ozone biases in CAM-chem in the Northern Hemisphere that have been attributed to excessive STE in the free-running version of CAM4, the low-top version of WACCM [*Tilmes et al.*, 2016]. As noted earlier, however, the values of $\overline{\chi}_{STE}$ are very small in the middle troposphere, suggesting that the differences in STE between the free-running simulations only contribute negligibly to the other (tropospheric) tracers.

4. Large-Scale Winds and Parameterized Convection

In order to interpret the transport differences discussed above we now compare the large-scale tropospheric circulation and parameterized convection between the simulations (Figures 3 and 4).

4.1. Comparisons Between MERRA and FR Simulations

The 500–700 hPa averaged zonal mean zonal winds are statistically identical between the four MERRA simulations (Figures 3a and 3c). This indicates that there are only small differences associated with how the dynamical

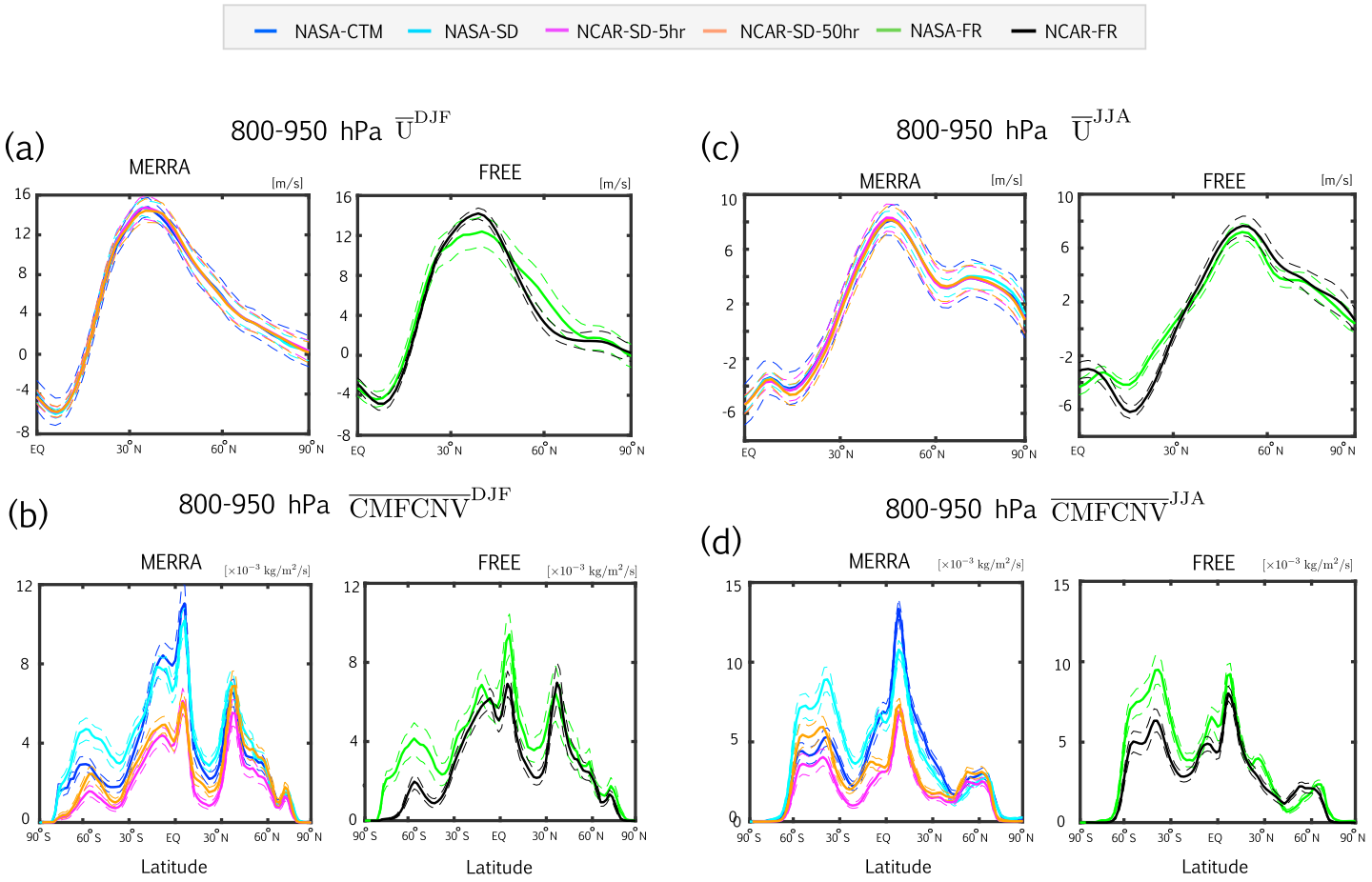

Figure 3. Latitudinal profiles of the zonally averaged climatological mean (a, b) DJF and (c, d) JJA zonal winds, averaged over 500–700 hPa (Figures 3a and 3c) and the 800–950 hPa averaged cumulative mass fluxes from convection, $\overline{CMFCNV}$ (Figures 3b and 3d). Left and right panels show comparisons between the MERRA constrained and free-running simulations, respectively. The coloring convention and indication of statistical significance (dashed lines) for the individual member of each suite is identical to the presentation in Figure 2.

fields are prescribed in the simulations, related either to errors incurred while interpolating between the MERRA analysis and the native model grid or from the way the large-scale flow is constrained to MERRA in the NASA-SD and NCAR-SD frameworks. Comparisons of maps of the zonal wind differences between the MERRA simulations also reveal statistically insignificant differences (not shown).

Differences in the zonally averaged winds between the FR simulations are larger, with weaker westerly winds over NH midlatitudes and weaker easterlies over the NH subtropics in the NASA-FR simulation, compared to the MERRA and the NCAR-FR simulations (Figures 3a and 3c). Note that over the NH subtropics the surface easterlies reflect low-level convergence associated with the lower branch of the Hadley circulation and, therefore, indicate that the mean meridional circulation in the NASA-FR simulation is slightly weaker than in the other runs throughout the year.

A comparison between lower tropospheric parameterized convection between the MERRA simulations reveals large differences between the NASA and NCAR simulations (Figures 3b and 3d). This is shown in terms of the seasonal mean 800–950 hPa averaged cumulative mass flux from convection ($\overline{CMFCNV}$) for DJF (Figure 3b) and JJA (Figure 3d), which reflects the seasonal migration of the Intertropical Convergence Zone into the NH during boreal summer. There are large differences in (parameterized) convection between the MERRA simulations during both seasons in the tropics and subtropics, where $\overline{CMFCNV}$ is nearly a factor of 2 larger in the NASA MERRA simulations. Maps of the 800–950 hPa averaged convective mass fluxes show that the large differences between the NASA MERRA and NCAR MERRA simulations in the subtropics and tropics are concentrated over the NH subtropical Pacific and Atlantic Oceans (Figure S1 in the supporting information). Note that while there are interesting differences between convection within each simulation

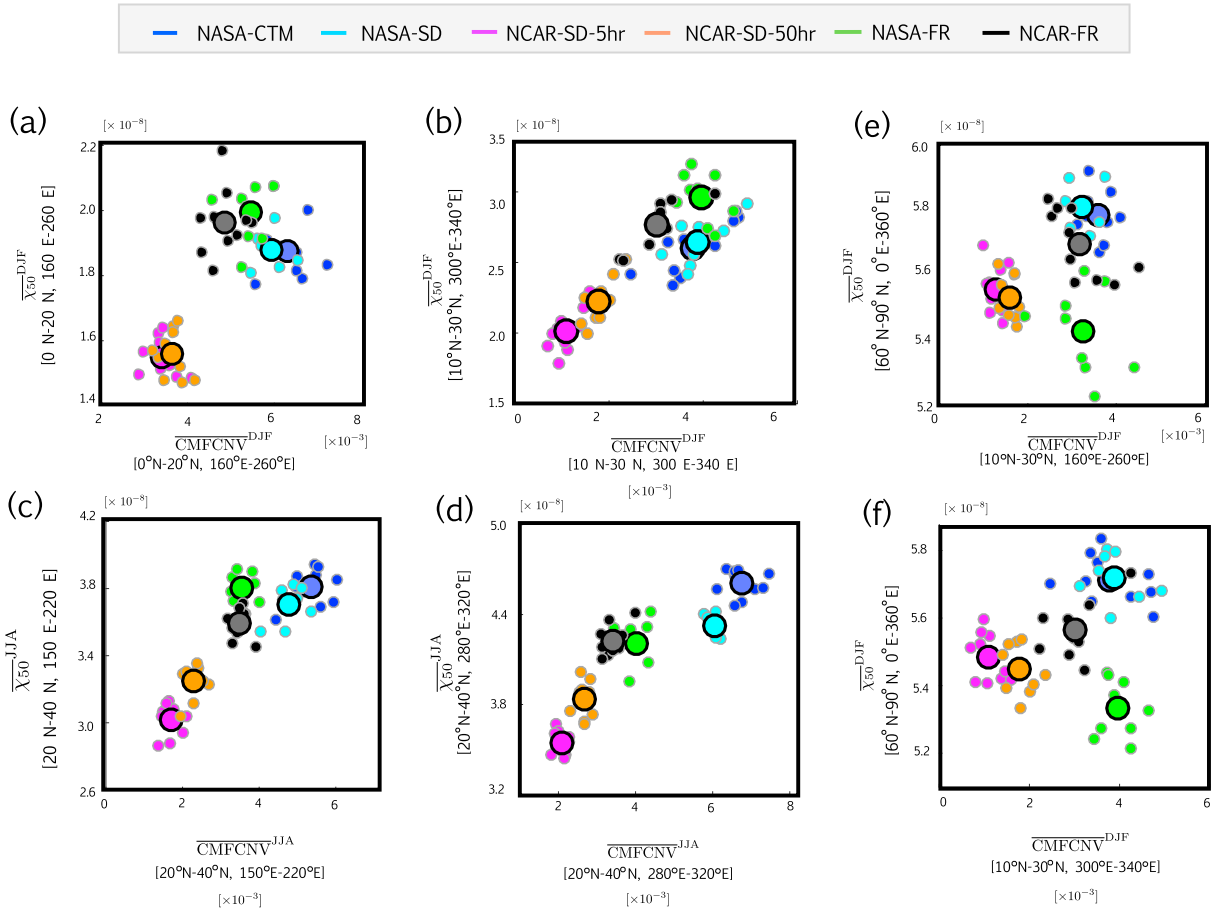

Figure 4. (a–d) Scatterplots showing strong local correlations between the 500–800 hPa averaged 50 day loss tracer concentration, $\overline{\chi_{50}}$, and the strength of parameterized convection in the lower troposphere, represented by the 800–950 mb averaged cumulative mass flux from convection, $\overline{\text{CMFCNV}}$, for DJF (Figures 4a, 4b, and 4e) and JJA (Figures 4c, 4d, and 4f). Spatial averages in Figures 4a–4d are performed over the Pacific and Atlantic. Scatterplots depicting strong remote correlations between the 500–800 hPa zonal mean 50 day loss tracer concentration, $\overline{\chi_{50}}$, at NH high latitudes and the strength of parameterized convection in the NH subtropical Pacific (Figure 4e) and Atlantic (Figures 4f) lower troposphere. The different colors correspond to individual simulations within the MERRA and FR suites, using the same color convention as in previous figures. Small circles correspond to individual years within the 2000–2009 climatological mean period, while large circles denote the climatological mean.

suite (e.g., NASA-CTM versus NASA-SD), these differences are significantly smaller than between the NASA and NCAR MERRA suites of runs. Furthermore, a comparison of the vertical profiles of $\overline{\text{CMFCNV}}$ between the simulations (not shown) indicates that the differences in convection occur at most levels throughout the lower troposphere so that the 500–800 mb column average captures the gross differences between the simulations.

In contrast to the MERRA simulations, there are relatively small differences in $\overline{\text{CMFCNV}}$ between the NASA and NCAR FR simulations (Figures 3b, 3d, and S1). The closer correspondence in parameterized convection in the NH subtropics between the NASA-FR and NCAR-FR simulations mainly reflects an increase in $\overline{\text{CMFCNV}}$ in the NCAR-FR simulation, compared to in the NCAR-SD simulations, e.g., the large increase in $\overline{\text{CMFCNV}}^{\text{JJA}}$ between 10°N and 30°N in the NCAR-FR simulation. Note that these differences are collocated with the subsiding branch of the Hadley circulation in the subtropics, suggesting that more work is needed to better understand the behavior of parameterized convection in regions of mean subsidence.

It is intriguing that the parameterized convection differences between the FR simulations are smaller than between the specified flow (MERRA) simulations. One possible explanation is that the convective mass fluxes in the NCAR-SD simulations, which are calculated by CAM column physics, are based on unbalanced meteorological fields in the case of the NCAR-FR simulation, versus balanced fields (i.e., the prescribed MERRA analysis) in the NCAR-SD simulations. More analysis of the relationship between parameterized convection and the

mean flow in simulations where the large-scale flow is prescribed, however, is beyond the scope of this study and will be explored in future work.

4.2. Transport Responses to Differences in Local and Remote Convection

To better relate differences in parameterized convection to transport differences between the MERRA simulations, we examine the relationship between the 50 day idealized loss tracer and lower tropospheric convection. Scatterplots of convection and 500–800 hPa averaged values of $\overline{\chi_{50}}$, evaluated over the subtropical oceans, show that for all simulations there is a strong linear relationship between the strength of parameterized convection in the tropics and subtropics and transport into the middle and upper troposphere for all years within the 2000–2009 climatological averaging period (Figure 4; see caption for details). Strong correlations between convection and transport hold for both the Pacific and Atlantic basins and for boreal winter and summer. Furthermore, despite, at times, large year-to-year natural variability, there is a clear separation between the NASA and NCAR MERRA suites of simulations that is statistically distinguishable for all basins and all seasons. Longitudinal cross sections of $\overline{\chi_5}$, $\overline{\chi_{50}}$, and the cumulative mass fluxes from convection for the individual MERRA simulations show in more detail the spatial extent of the relationship between oceanic convection and transport aloft (not shown; Figures S2 and S3).

Finally, the larger values of $\overline{\chi_5}^{DJF}$ and $\overline{\chi_{50}}^{DJF}$ in the NASA MERRA simulations that occur poleward of Ω_{MID} indicate that differences in subtropical convection can also impact remote transport to high latitudes. More precisely, stronger parameterized convection in the NH subtropics can enhance the lifting of air parcels that are labeled on the southern edge of Ω_{MID} onto potential temperature surfaces that extend poleward to the high-latitude upper troposphere ($\theta > \sim 290$ K). Scatterplots of the 800–950 hPa averaged surface convective mass flux over the NH subtropics and the middle tropospheric 60°N–90°N zonally averaged values of $\overline{\chi_{50}}^{DJF}$ (Figures 4e and 4f) show that this relationship holds for all years in the climatology, over both Pacific and Atlantic basins and for nearly all of the simulations. Interestingly, this relationship is noticeably absent in the NASA-FR simulation and may be related to the large biases in the large-scale flow, in which $\overline{U}^{DJF}$ is significantly weaker relative to both the NCAR-FR simulation and MERRA (Figure 3a). More work is needed to better understand how these tropical convection and high-latitude transport relationships depend on various aspects of the mean circulation but is beyond the scope of the current study.

5. Conclusions

Our main goal in this study has been to compare large-scale tropospheric transport between models that use the same meteorological fields. Our main conclusions are the following:

1. Models that use the same specified large-scale dynamical fields can produce very different tropospheric transport. Here we find that the mean age in the Southern Hemisphere differs by more than 0.5 years (or ~25–30%) between simulations driven with MERRA meteorological fields.
2. The transport differences between the MERRA simulations are not related to how the large-scale flow is specified—be it directly from the analysis (as in a CTM) or prescribed online (as in a nudged simulation)—but, rather, are due to differences in parameterized convective transport between the models.
3. The transport differences between free-running versions of models is smaller than differences between simulations constrained to use the same large-scale flow. This is because parameterized convection in the free-running simulations is more similar than between the MERRA constrained simulations.

The fact that the differences in transport between constrained versions of the NASA and NCAR models is larger than differences between their corresponding free-running simulations (which have differing large-scale flow) suggests that extra caution should be taken when interpreting differences in tropospheric composition between models that use the same meteorology. Our results indicate that more attention needs to be paid to understanding the coupling between (parameterized) convection with the large-scale flow and, in particular, the details of how convection is calculated in simulations where the meteorological fields are prescribed. Furthermore, they suggest that there may only be limited validity in using simulations in which the meteorological fields are prescribed to assess the impact of meteorology on trends.

One way to further examine the impacts of parameterized convection on transport is to perform simulations where transport by the convective mass fluxes is turned off [*Lawrence et al.*, 2003; *Doherty et al.*, 2005], even though this poses difficulties in interpretation as it ignores the component of convection that occurs in the large-scale flow via the Hadley circulation [*Lawrence and Salzmann*, 2008]. Alternative approaches,

such as that described in *Hess* [2005], by which moist convectively processed tracers are tagged according to when and where they last encounter convection, may provide a more natural framework for exploring these issues further.

Before concluding, one caveat must be discussed. Namely, our study focuses mainly on parameterized convection differences over the tropical and subtropical oceans, as these are most responsible for the large transport differences between the MERRA simulations. Therefore, the results from this study have the largest implications for the modeling of trace gases and aerosols that have oceanic sinks and sources or, for pure anthropogenic tracers, are long-lived enough that they respond to transport over the oceans. Thus, we expect that our results will have important implications for constituents including the broad range of short-living ozone-depleting species that are emitted over the oceans, which will be very sensitive to different representations of subtropical convection [*Hossaini et al.*, 2016]. We will explore this in detail using both idealized and chemical tracer output from the suite of models participating in CCMI.

Acknowledgments
The authors thanks useful discussions with Andrea Molod and the high-performance computing resources provided by NASA's Advanced Supercomputing (NAS) Division and the NASA Center for Climate Simulation (NCCS). D.W. acknowledges support from NSF grant AGS-1403676 and NASA grant NNX14AP58G. The National Center for Atmospheric Research (NCAR) is sponsored by the U.S. National Science Foundation. WACCM is a component of the Community Earth System Model (CESM), which is supported by the National Science Foundation (NSF) and the Office of Science of the U.S. Department of Energy. Computing resources were provided by NCAR's Climate Simulation Laboratory, sponsored by NSF and other agencies. This research was enabled by the computational and storage resources of NCARÕs Computational and Information Systems Laboratory (CISL). All data and model output used in this study are available by contacting the corresponding author (clara.orbe@nasa.gov).

References

Bloom, S., L. Takacs, A. Da Silva, and D. Ledvina (1996), Data assimilation using incremental analysis updates, *Mon. Weather Rev.*, *124*(6), 1256–1271.

Colarco, P., A. da Silva, M. Chin, and T. Diehl (2010), Online simulations of global aerosol distributions in the NASA GEOS-4 model and comparisons to satellite and ground-based aerosol optical depth, *J. Geophys. Res.*, *115*, D14207, doi:10.1029/2009JD012820.

Doherty, R., D. Stevenson, W. Collins, and M. Sanderson (2005), Influence of convective transport on tropospheric ozone and its precursors in a chemistry-climate model, *Atmos. Chem. Phys.*, *5*(12), 3205–3218.

Eyring, V., et al. (2013), Overview of IGAC/SPARC Chemistry-Climate Model Initiative (CCMI) community simulations in support of upcoming ozone and climate assessments, *SPARC Newslett.*, *40*, 48–66.

Geller, L., J. Elkins, J. M. Lobert, A. Clarke, D. Hurst, J. Butler, and R. Myers (1997), Tropospheric SF6: Observed latitudinal distribution and trends, derived emissions and interhemispheric exchange time, *Geophys. Res. Lett.*, *24*, 675–678.

Gilliland, A., and D. Hartley (1998), Interhemispheric transport and the role of convective parameterizations, *J. Geophys. Res.*, *103*(D17), 22,039–22,045.

Hack, J. J. (1994), Parameterization of moist convection in the National Center for Atmospheric Research Community Climate Model (CCM2), *J. Geophys. Res.*, *99*(D3), 5551–5568.

Hess, P. (2005), A comparison of two paradigms: The relative global roles of moist convective versus nonconvective transport, *J. Geophys. Res.*, *110*, D20302, doi:10.1029/2004JD005456.

Hossaini, R., et al. (2016), A multi-model intercomparison of halogenated very short-lived substances (TransCom-VSLS): Linking oceanic emissions and tropospheric transport for a reconciled estimate of the stratospheric source gas injection of bromine, *Atmos. Chem. Phys. Discuss.*, *16*, 9163–9187.

Klonecki, A., P. Hess, L. Emmons, L. Smith, J. Orlando, and D. Blake (2003), Seasonal changes in the transport of pollutants into the Arctic troposphere-model study, *J. Geophys. Res.*, *108*(D4), 8367, doi:10.1029/2002JD002199.

Kunz, A., L. Pan, P. Konopka, D. Kinnison, and S. Tilmes (2011), Chemical and dynamical discontinuity at the extratropical tropopause based on START08 and WACCM analyses, *J. Geophys. Res.*, *116*, D24302, doi:10.1029/2011JD016686.

Lawrence, M., and M. Salzmann (2008), On interpreting studies of tracer transport by deep cumulus convection and its effects on atmospheric chemistry, *Atmos. Chem. Phys.*, *8*(20), 6037–6050.

Lawrence, M. G., R. von Kuhlmann, M. Salzmann, and P. J. Rasch (2003), The balance of effects of deep convective mixing on tropospheric ozone, *Geophys. Res. Lett.*, *30*(18), 1940, doi:10.1029/2003GL017644.

Levin, I., and V. Hesshaimer (1996), Refining of atmospheric transport model entries by the globally observed passive tracer distributions of 85krypton and sulfur hexafluoride (SF6), *J. Geophys. Res.*, *101*(D11), 16,745–16,755.

Marsh, D. R., M. J. Mills, D. E. Kinnison, J.-F. Lamarque, N. Calvo, and L. M. Polvani (2013), Climate change from 1850 to 2005 simulated in CESM1 (WACCM), *J. Clim.*, *26*(19), 7372–7391.

Meijer, E. W., B. Bregman, A. Segers, and P. F. van Velthoven (2004), The influence of data assimilation on the age of air calculated with a global chemistry-transport model using ECMWF wind fields, *Geophys. Res. Lett.*, *31*, L23114, doi:10.1029/2004GL021158.

Molod, A., L. Takacs, M. Suarez, J. Bacmeister, I.-S. Song, and A. Eichmann (2012), The GEOS-5 Atmospheric General Circulation Model: Mean climate and development from MERRA to Fortuna.

Moorthi, S., and M. J. Suarez (1992), Relaxed Arakawa-Schubert. A parameterization of moist convection for general circulation models, *Mon. Weather Rev.*, *120*(6), 978–1002.

Morgenstern, O., et al. (2016), Review of the global models used within the Chemistry-Climate Model Initiative (CCMI), *Geos. Mod. Dev.*, doi:10.5194/gmd-2016-199.

Orbe, C., M. Holzer, L. M. Polvani, and D. Waugh (2013), Air-mass origin as a diagnostic of tropospheric transport, *J. Geophys. Res. Atmos.*, *118*, 1459–1470, doi:10.1002/jgrd.50133.

Orbe, C., P. A. Newman, D. W. Waugh, M. Holzer, L. D. Oman, F. Li, and L. M. Polvani (2015), Air-mass origin in the Arctic part II: Response to increases in greenhouse gases, *J. Clim.*, *28*(23), 9105–9120.

Orbe, C., D. W. Waugh, P. A. Newman, and S. Steenrod (2016), The transit-time distribution from the Northern Hemisphere midlatitude surface, *J. Atmos. Sci.*, *73*, 3785–3802.

Ott, L., S. Pawson, and J. Bacmeister (2011), An analysis of the impact of convective parameter sensitivity on simulated global atmospheric CO distributions, *J. Geophys. Res.*, *116*, D21310, doi:10.1029/2011JD016077.

Patra, P. K., et al. (2011), *Atmos. Chem. Phys.*, *11*(24), 12,813–12,837.

Pawson, S., I. Stajner, S. R. Kawa, H. Hayashi, W.-W. Tan, J. E. Nielsen, Z. Zhu, L.-P. Chang, and N. J. Livesey (2007), Stratospheric transport using 6-h-averaged winds from a data assimilation system, *J. Geophys. Res.*, *112*, D23103, doi:10.1029/2006JD007673.

Prather, M. J., X. Zhu, Q. Tang, J. Hsu, and J. L. Neu (2011), An atmospheric chemist in search of the tropopause, *J. Geophys. Res.*, *116*, D04306, doi:10.1029/2010JD014939.

Rayner, N., D. E. Parker, E. Horton, C. Folland, L. Alexander, D. Rowell, E. Kent, and A. Kaplan (2003), Global analyses of sea surface temperature, sea ice, and night marine air temperature since the late nineteenth century, *J. Geophys. Res.*, *108*(D14), 4407, doi:10.1029/2002JD002670.

Rienecker, M. M., et al. (2011), MERRA: NASA's modern-era retrospective analysis for research and applications, *J. Clim.*, *24*(14), 3624–3648.

Rind, D., J. Lerner, J. Jonas, and C. McLinden (2007), Effects of resolution and model physics on tracer transports in the NASA Goddard Institute for Space Studies general circulation models, *J. Geophys. Res.*, *112*, D09315, doi:10.1029/2006JD007476.

Saito, R., et al. (2013), TransCom model simulations of methane: Comparison of vertical profiles with aircraft measurements, *J. Geophys. Res. Atmos.*, *118*, 3891–3904, doi:10.1002/jgrd.50380.

Schoeberl, M. R., A. R. Douglass, Z. Zhu, and S. Pawson (2003), A comparison of the lower stratospheric age spectra derived from a general circulation model and two data assimilation systems, *J. Geophys. Res.*, *108*(D3), 4113, doi:10.1029/2002JD002652.

Scinocca, J. F., and N. A. McFarlane (2004), The variability of modeled tropical precipitation, *J. Atmos. Sci.*, *61*(16), 1993–2015.

Stohl, A. (2006), Characteristics of atmospheric transport into the Arctic troposphere, *J. Geophys. Res.*, *111*, D11306, doi:10.1029/2005JD006888.

Strahan, S., B. Duncan, and P. Hoor (2007), Observationally derived transport diagnostics for the lowermost stratosphere and their application to the GMI chemistry and transport model, *Atmos. Chem. Phys.*, *7*(9), 2435–2445.

Strode, S., B. Duncan, E. Yegorova, J. Kouatchou, J. Ziemke, and A. Douglass (2015), Implications of carbon monoxide bias for methane lifetime and atmospheric composition in chemistry climate models, *Atmos. Chem. Phys.*, *15*(20), 11,789–11,805, doi:10.5194/acp-15-11789-2015.

Suarez, M. J., et al. (2008), The GEOS-5 data assimilation system—Documentation of versions 5.0. 1, 5.1. 0, and 5.2.0.

Tilmes, S., et al. (2016), Representation of the Community Earth System Model (CESM1) CAM4-chem within the Chemistry-Climate Model Initiative (CCMI), *Geosci. Model Dev.*, *9*(5), 1853–1890.

Waugh, D., et al. (2013), Tropospheric SF6: Age of air from the Northern Hemisphere midlatitude surface, *J. Geophys. Res. Atmos.*, *118*(19), 11–429.

Zhang, G. J., and N. A. McFarlane (1995), Sensitivity of climate simulations to the parameterization of cumulus convection in the Canadian Climate Centre general circulation model, *Atmosphere-Ocean*, *33*(3), 407–446.